Optical Control of Plasmonic Bloch Modes on Periodic Nanostructures

B. Gjonaj,*[,†] J. Aulbach,[†] P. M. Johnson,[†] A. P. Mosk,[‡] L. Kuipers,[†] and A. Lagendijk[†]

[†]FOM-Institute for Atomic and Molecular Physics AMOLF, Science Park 104, 1098 XG Amsterdam, The Netherlands

[‡]Complex Photonic Systems, Faculty of Science and Technology, and MESA+ Institute for Nanotechnology, University of Twente, P.O. Box 217, 7500 AE Enschede, The Netherlands

ABSTRACT: We study and actively control the coherent properties of surface plasmon polaritons (SPPs) optically excited on a nanohole array. Amplitude and phase of the optical excitation are externally controlled via a digital spatial light modulator (SLM) and SPP interference fringe patterns are designed and observed with high contrast. Our interferometric observations reveal SPPs dressed with the Bloch modes of the periodic nanostructure. The momentum associated with these dressed plasmons (DP) is highly dependent on the grating period and fully matches our theoretical predictions. We show that the momentum of DP waves can, in principle, exceed the SPP momentum. Actively controlling DP waves via programmable phase patterns offers the potential for high field confinement applicable in lithography, surface enhanced Raman scattering, and plasmonic structured illumination microscopy.

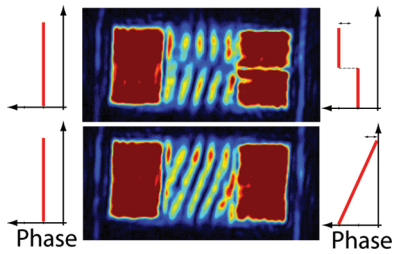

KEYWORDS: *Plasmonics, wavefront shaping, interferometry, microscopy, Bloch modes*

Important systems, such as biological cells, single molecules, and nanodevices, strongly interact with visible light on subwavelength scales. Yet, standard microscopy and related applications in lithography, sensing, and imaging are diffraction limited. Plasmonics[1] offers an alternative route to control light with subwavelength precision through the excitation of surface plasmon polaritons (SPPs).[2,3] These surface waves, bound to a metal dielectric interface, are a hybrid mode of photons and electronic change-density oscillations. The intrinsic momentum associated with these evanescent waves is higher than that of free propagating photons. Thus, for a fixed light frequency SPPs have a higher effective refractive index and tighter confinement of electromagnetic energy.[4]

Achieving the full promise of SPPs in applications requires two types of innovation, (1) subwavelength confinement and (2) flexible control. Confinement has been achieved via tailored samples that allow plasmonic waves to be coupled into the topological modes of a fabricated structure. This mode can be referred to as a dressed plasmon (DP) because the propagation is determined by the nanostructure. Successful confining geometries include coupled nanoantennas[5−7] that fully localize modes in the gap between neighboring antennas and V-grooved[8,9] and nanowire[10,11] waveguides that support one-dimensional (1D) propagating modes deeply confined inside the waveguide. The field confinement in such geometries exceeds that of freely propagating SPPs by an order of magnitude. Flexible control has been partially achieved in several very recent experiments.[12−14] These and similar experiments achieve control of propagating SPPs via a single parameter such as the polarization state, the angle, or the wavelength.

Theoretical works have shown that it is possible to take confinement and flexible control much further. For example, it has been theoretically suggested to use nanostructures,[15,16] such as well designed gratings,[17] to support extended DP waves to obtain both high confinement (and thus resolution) and flexible control over a large field of view.[18,19] Experimental implementation of this kind of flexible approach would open the door to appplications such as plasmon-based saturated structured illumination microscopy (SSIM)[20] and related applications in imaging,[21,22] sensing,[23] and lithography.[24]

In this paper, we are not only able to generate Bloch mode dressed plasmons supported by periodic nanostructures but also obtain full flexible optical control over these modes via plasmonic phase imprint.[25,26] Using a spatial light modulator (SLM) we shape the amplitude and phase profile of the incident laser beam over a large 2D field of view. The SLM is imaged onto the surface of the sample, thus addressing each pixel of the SLM (the control parameters) to a corresponding area on the sample. We use the amplitude control to measure with high contrast fringe patterns generated from two counter propagating SPP waves. The momentum associated with the standing waves shows strong dependence on the lattice period of the grating and reveals the Bloch-mode dressing of the surface plasmons. Furthermore, we use the phase control to shape the interference pattern at will. As an example of such phase control, we chose to deterministically scan and tilt the fringe pattern of the dressed plasmons as required for a plasmonic analogue of structured illumination microscopy.

A diagram of the setup is given in Figure 1. The SLM is imaged on the sample via a lens (L_1) and the objective, referred

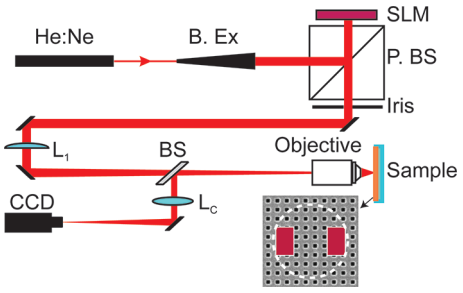

Figure 1. Experimental setup. Linearly polarized light from a HeNe laser is first expanded by a beam expander (B. Ex) and sent to the spatial light modulator (SLM). A polarizing beam splitter (P. BS) filters only the cross-polarized component of the SLM's reflection. The SLM is imaged point to point onto the sample (a nanoperforated gold film on glass) via the imaging system (lens L_1, objective). The sample is in the objective's focal plane of the with the gold side toward it (where the SLM image is created). The reflection from the sample is imaged point to point onto the CCD camera (objective, lens L_C). Inset: Sample illuminated with structured amplitude from the SLM. The white dashed ring indicates the SLM perimeter while the red blobs indicate SLM segments set to nonzero amplitude.

to hereafter together as the imaging system. The SLM is at the focal plane of lens L_1 (focal length 130 cm). The image at infinity created by L_1 is projected onto the sample at the focal plane of the objective. Our SLM (Holoeye LC-R 720) is a reflective display based on twisted nematic liquid crystal on silicon technology. The display has a total of 1280 × 768 pixels operating at 60 Hz with a response time of 3 ms. Each pixel is 20 μm in size and addressed with a 8-bit voltage. The objective (Nikon LU PLAN FLUOR P 100X) is infinity corrected and metallurgic (no coverslip compensation) with a Numerical Aperture (NA) of 0.9 and a magnification of 100 times (defined for a tube lens of 20 cm focal length). The focal length of L_1 is 6.5 times larger than that of the standard tube lens yielding a corresponding 650 times demagnification of the image. The distance between L_1 and the objective is 1 m, that is, shorter than the focal length of L_1 (nontelecentric imaging system). In this configuration the average angle of illumination is position dependent, which is an important condition for the SPPs launching.

The light emitted in reflection from the sample is imaged on the CCD (AVT Dolphin F145 B) using lens L_C as tube lens. This light includes both the direct reflection of the illuminating beam and the scattered light from SPPs. Thus, the resulting image is a combination of both the SLM amplitude pattern and the generated SPP pattern. To distinguish between the two we choose illumination patterns that allow SPP observation in a nonilluminated area. The amplitude and phase of the excitation pattern is controlled by applying the 4-pixel technique[27] to the SLM. Four adjacent pixels are grouped into a superpixel by selecting a first diffractive order with the neighbor-pixel fields being $\pi/4$ out of phase. In this work, we use 32 × 32 superpixels. Every SLM superpixel is imaged on a sample area of 440 × 440 nm^2 containing nearly one unit cell of the grating. Such a superpixel grouping provides continuous modulation over full amplitude ($A \in [0, 1]$) and phase ($\Phi \in [0, 2\pi]$) ranges with a cross modulation of less than 1%.

Our samples, nanohole arrays similar to those used typically for enhanced optical transmission experiments, were fabricated using focused ion beam milling. A 200 nm gold film was deposited on top of 1 mm BK7 glass substrate with a 2 nm chromium adhesion layer. Square holes were milled with sides of 177 nm. The hole array covers an area of 30 × 30 μm^2. Five samples were fabricated with array periods (a_0) varying from 350 to 450 nm. The sample was placed with the gold side toward the objective to observe SPP waves from the gold−air interface. We calculate the SPP momentum for incident radiation of λ_0 = 633 nm ($k_0 = 2\pi/\lambda_0$) using tabulated values[28] of the dielectric constants of gold ε_m and air ε_d

$$k_S = k_0 \mathrm{Re}\sqrt{\frac{\varepsilon_m \varepsilon_d}{\varepsilon_m + \varepsilon_d}} = (m, n)k_G + k_0 \sin\theta \quad (1)$$

where the last equality expresses the fact that the SPP momentum is a vectorial sum of the $(m,n)k_G$ grating orders ($k_G = 2\pi/a_0$) and the in-plane component of the incident light. With our oblique illumination scheme, the average angle of incidence θ is not uniform but position dependent.

This illumination scheme and its role on how SPPs are launched is illustrated in Figure 2. Each SLM's superpixel is

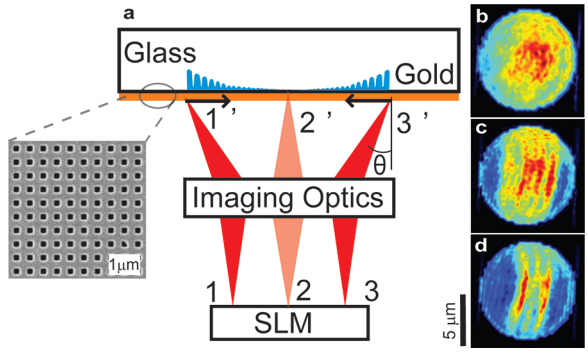

Figure 2. (a) Sketch of the sample illumination. Each SLM point is imaged on the surface of the sample with a different average angle of incidence θ. (b−d) Reflection from different samples illuminated with a uniform amplitude and phase profile. (b) On the bare gold sample the reflection is also uniform since no SPPs are launched. Deviations from a truncated Gaussian profile are due to surface roughness. (c) The dark areas of low reflection from the 400 nm hole array indicate the angular (spatial) bands for SPP launching. (d) These bands are sample dependent as shown for the 425 nm hole array. Inset: SEM image of the samples.

projected onto the sample with a different average angle of incidence (Figure 2a) and thus with a different in-plane component of the incident light. The momentum conservation described in eq 1 will be satisfied only within specific angular bands that are position dependent. In Figure 2b−d, we show the surface of three different samples illuminated with a uniform amplitude profile across the SLM with horizontal polarization.

For the reference bare gold film and a uniform SLM amplitude and phase profile, the reflected image is nearly identical to incident beam profile since no SPP can be launched (Figure 2b). Corrugations on the bare metal film (due to polycrystalline gold) give rise to a speckle pattern on top of the truncated (80%) Gaussian profile. When the same uniform amplitude and phase profile is projected onto a nanohole array, dark and bright areas are clearly distinguishable as shown in

Figure 2c,d. Dark areas correspond to suppressed reflection from the sample. We interpret these dark areas as the spatial (angular) bands that satisfy eq 1 and thus where plasmons are efficiently excited from the incident light. The location of these bands strongly depends on the array momentum. Even a 25 nm variation of the array period from a_0 = 425 nm (Figure 2c) to a_0 = 400 nm (Figure 2d) yields a spatial band shift of nearly 2 μm.

SPPs waves launched in the momentum matched bands propagate toward each other and interfere (Figure 2). Yet this interference pattern is observed on a high background due to the direct reflection of the incident light. To remove the background and enhance the contrast of the SPP interference pattern we spatially design the incident amplitude profile with "on" areas of amplitude A = 1 and an "off" background of A = 0. Each "on" area is composed of 10 × 8 superpixels and is located in the vicinity of the two symmetric angular bands. The SPP interference patterns are then observed in the central non-illuminated area, which is our SPP field of view.

Results from this designed amplitude profile are shown in Figure 3. When the two counterpropagating SPP waves

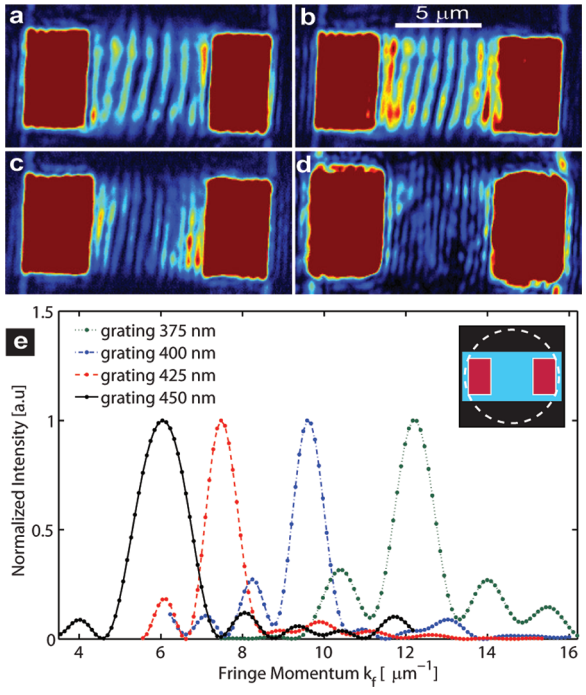

Figure 3. SPP fringe formation via counter propagating waves. The image geometry and the incident amplitude profile are shown in the inset. The polarization of the incident light is horizontal. (a–d) We observe different fringe patterns for array periods of 375 (a), 400 (b), 425 (c), and 450 (d). In (e) are shown the line Fourier transforms of these fringe patterns.

launched in the on areas interfere, a standing wave pattern of intensity is created. For SPPs propagating on an ideally smooth and noncorrugated sample, we expect the period of the fringe pattern to be half the SPP wavelength ($\lambda_S = 2\pi/k_S$ = 590 nm). Instead, the measured fringe period is found to be sample dependent (Figure 3a–d). We measured fringe periods P of 1 ± 0.05, 0.85 ± 0.05, 0.65 ± 0.05, 0.5 ± 0.05, and 0.45 ± 0.05 μm for grating pitches of 450, 425, 400, 375, and 350 nm, respectively. The different filling fractions of our samples, which perturb the SPP wavelength within few percent, can not explain the large deviations we observe.

We attribute the fringe patterns to a mixing of the original SPP wave with the hole array.[29] We can analyze the results using a one-dimensional model because for all our samples we observe only horizontal propagation. Theoretically there are two ways to mix SPPs with the hole array: intensity mixing (expected for incoherent forms of scattering such as fluorescence) and field convolution (expected for coherent scattering processes). We will discuss both ways even though the experimental observations confirm only the field convolution. We first consider intensity convolution. An SPP standing intensity pattern with momentum $2k_S$ is formed, but because we observe the pattern through the scattering of a periodic structure with momentum k_G, the fringe momentum appears to be $2k_S \pm k_G$. This intensity convolution does not match the experimental observations. The situation is completely different for the field convolution. The hybridization of the bare SPPs with the Bloch modes of the array results in dressed plasmonic (DP) waves of momentum $k_S + mk_G$ (m integer). These DP waves then result in standing intensity patterns of momentum $2(k_S + mk_G)$.

A comparison between experiment and the amplitude convolution approach for these DP waves is shown in Figure

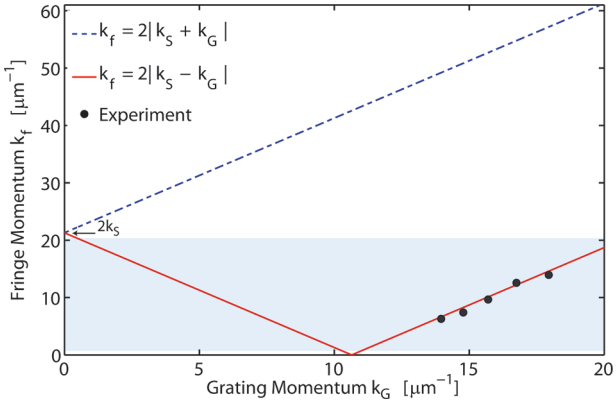

Figure 4. SPP fringe momentum versus the grating momentum. The experimental data shows SPPs convoluted with the m = −1 Bloch mode of the arrays. The other Bloch modes can not be resolved due to limited detection bandwidth (light blue square).

4. The modulus of the fringe momentum (k_f) is plotted against the modulus of the grating momentum (k_G). The two lines are the theoretical predictions for SPPs convolved with the first positive (m = 1) and the first negative (m = −1) grating orders. The experimental data perfectly follow only the m = −1 curve. The first positive order is not observed in our far-field measurement due to its evanescent nonradiative nature and the limited resolution of our setup. The distribution of fringe momenta can be expressed except for a normalization factor as

$$P_f(k) = B(k) \sum_{m \in \mathbb{Z}} \eta_m \delta(k - 2|k_S + mk_G|) \qquad (2)$$

where every δ represents the standing pattern from one of the m orders of the array, η_m represents the coupling efficiency of SPPs into this m^{-th} order, and $B(k)$ is the momentum bandwidth of our detection optics. Our bandwidth is shown as the light blue rectangle in Figure 4 and we approximate it with a step function limited by the optical diffraction limit and the SPP field of view (the distance between the two "on" areas). Upon inserting this bandwidth in eq 2 only SPP hybridization

with the $m = -1$ term survives because all other DP modes have fringe momentum that exceeds the diffraction limit.

Finally, in Figure 5 we show phase control of the propagating Bloch-mode dressed SPPs. As an important example, we chose

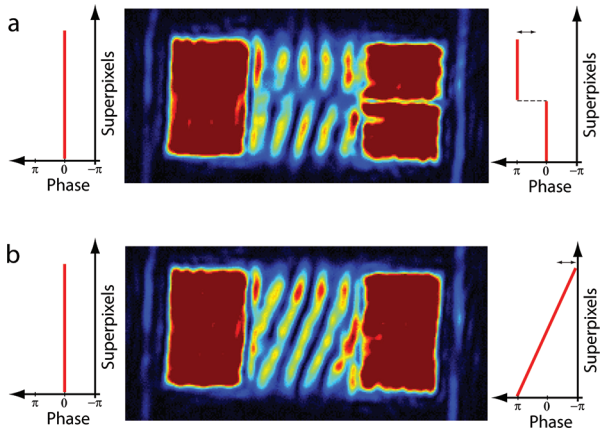

Figure 5. Scanning the fringes by phase tuning. (a) The phase of the left on area is kept constant while the phase of the right on area has a step jump between the lower and upper part as shown in the wings of the figure. The resulting fringe pattern in the upper part is shifted compared to the lower one. (b) The fringes are rotated due to a linearly incrementing phase on the right on area.

to scan and tilt the fringe pattern in a deterministic approach as required for a plasmonic analog of structured illumination microscopy. Furthermore in this analogy, the predicted high momentum Bloch modes will act as the nonlinear terms of saturated structured illumination microscopy.

We can scan the fringe pattern across the sample by varying the phase delay between the two "on" areas and thus introducing an optical retardation that will translate the DP fringes. We experimentally prove this phase scanning principle for the $m = -1$ DP modes as shown in Figure 5a where the upper half of the right "on" area is out of phase with the rest of the illuminated areas. The different phase delays result in a translated fringe pattern in the upper part. The line scan resolution (fringe translation) is given by our digital phase control: 256 steps from 0 to 2π phase delay. As an alternative, by applying a linear phase difference between the two "on" areas, the standing pattern will result in tilted plasmonic fringes (angular scan) as shown in Figure 5b.

The predicted presence of the $m = 1$ DP mode, which represents a sub-100 nm period intensity beating on top of the observed fringe pattern, combined with our ability to scan the pattern across the sample, suggest interesting prospects for subwavelength imaging. Because of the very weak signal of the mode (relative to $m = -1$) and to the diffraction limit we cannot resolve this fast beating in the current experimental configuration. However it should be possible, using near field imaging and optimizing the sample for a maximal value of $\eta_{m=1}$, to calibrate this sub-100 nm intensity pattern for different fringe patterns (line and angular scans). Once calibrated, the sample surface could be used to image sub-100 nm objects with only far field probing and image correlations.

We have shown here the observation of Bloch-mode dressed surface plasmon polaritons (DP) propagating on nanohole arrays of different subwavelength periodicities. We recorded the standing intensity pattern of two counterpropagating DP waves. The dependence of the measured fringe period on the period of the nanostructure is perfectly described by a simple model of plasmonic Bloch mode interference. By actively imposing well-programmed phase relations to these plasmonic Bloch modes, we achieved full and all optical control of their interference patterns. Bloch dressed SPPs are 2D propagating waves that can achieve high momentum and thus actively controlling their interference patterns has potential for lithography, super-resolution biosensing and imaging applications.

AUTHOR INFORMATION

Corresponding Author

*E-mail: b.gjonaj@amolf.nl.

Notes

The authors declare no competing financial interest.

ACKNOWLEDGMENTS

We thank Hans Zeijlermaker and Dimitry Lamers for sample fabrication. This work is part of the research program of the "Stichting voor Fundamenteel Onderzoek der Materie", which is financially supported by the "Nederlandse Organisatie voor Wetenschappelijk Onderzoek".

REFERENCES

(1) Barnes, W. L.; Dereux, A.; Ebbesen, T. W. *Nature* **2003**, *424*, 824−830.
(2) Ozbay, E. *Science* **2006**, *311*, 189.
(3) Polman, A. *Science* **2008**, *322*, 868.
(4) Schuller, J. A.; Barnard, E. S.; Cai, W.; Jun, Y. C.; White, J. S.; Brongersma, M. L. *Nat. Mater.* **2010**, *9*, 193.
(5) Schuck, P. J.; Fromm, D. P.; Sundaramurthy, A.; Kino, G. S.; Moerner, W. E. *Phys. Rev. Lett.* **2005**, *94*, 017402.
(6) Mühlschlegel, P.; Eisler, H. J.; Martin, O. J. F.; Hecht, B.; Pohl, D. W. *Science* **2005**, *308*, 1607−1609.
(7) Novotny, L.; van Hulst, N. *Nat. Photonics* **2011**, *5*, 83−90.
(8) Søndergaard, T.; Bozhevolnyi, S. I.; Beermann, J.; Novikov, S. M.; Devaux, E.; Ebbesen, T. W. *Nano Lett.* **2010**, *10*, 291−295.
(9) Stockman, M. I. *Phys. Rev. Lett.* **2004**, *93*, 137404.
(10) Krenn, J. R.; Lamprecht, B.; Ditlbacher, H.; Schider, G.; Salerno, M.; Leitner, A.; Aussenegg, F. R. *Europhys. Lett.* **2002**, *60*, 663.
(11) Verhagen, E.; Spasenović, M.; Polman, A.; Kuipers, L. K. *Phys. Rev. Lett.* **2009**, *102*, 203904.
(12) Benetou, M. I.; Thomsen, B. C.; Bayvel, P.; Dickson, W.; Zayats, A. V. *Appl. Phys. Lett.* **2011**, *98*, 111109.
(13) Stein, B.; Laluet, J.; Devaux, E.; Genet, C.; Ebbesen, T. W. *Phys. Rev. Lett.* **2010**, *105*, 266804.
(14) Feng, L.; Mizrahi, A.; Zamek, S.; Liu, Z.; Lomakin, V.; Fainman, Y. *ACS Nano* **2011**, *5*, 5100−5106.
(15) Volpe, G.; Molina-Terriza, G.; Quidant, R. *Phys. Rev. Lett.* **2010**, *105*, 216802.
(16) Kao, T. S.; Jenkins, S. D.; Ruostekoski, J.; Zheludev, N. I. *Phys. Rev. Lett.* **2011**, *106*, 085501.
(17) Rodrigo, S. G.; Mahboub, O.; Degiron, A.; Genet, C.; García-Vidal, F. J.; Martín-Moreno, L.; Ebbesen, T. W. *Opt. Express* **2010**, *18*, 23691−23697.
(18) Sentenac, A.; Chaumet, P. C. *Phys. Rev. Lett.* **2008**, *101*, 013901.
(19) Bartal, G.; Lerosey, G.; Zhang, X. *Phys. Rev. B* **2009**, *79*, 201103.
(20) Gustafsson, M. G. L. *Proc. Natl. Acad. Sci. U.S.A.* **2005**, *102*, 13081−13086.
(21) Ozaki, M.; ichi Kato, J.; Kawata, S. *Science* **2011**, *332*, 218−220.
(22) Wei, F.; Liu, Z. *Nano Lett.* **2010**, *10*, 2531−2536.
(23) Koller, D. M.; Hohenester, U.; Hohenau, A.; Ditlbacher, H.; Reil, F.; Galler, N.; Aussenegg, F. R.; Leitner, A.; Trügler, A.; Krenn, J. R. *Phys. Rev. Lett.* **2010**, *104*, 143901.
(24) Kravchenko, A.; Shevchenko, A.; Ovchinnikov, V.; Priimagi, A.; Kaivola, M. *Adv. Mater.* **2011**, *23*, 4174−4177.

(25) Gjonaj, B.; Aulbach, J.; Johnson, P. M.; Mosk, A. P.; Kuipers., L.; Lagendijk, A. *Nat. Photonics* **2011**, *5*, 360−363.
(26) Zhang, P.; Wang, S.; Liu, Y.; Yin, X.; Lu, C.; Chen, Z.; Zhang, X. *Opt. Lett.* **2011**, *36*, 3191−3193.
(27) van Putten, E. G.; Vellekoop, I. M.; Mosk, A. P. *Appl. Opt.* **2008**, *47*, 2076.
(28) Johnson, P. B.; Christy, R. W. *Phys. Rev. B* **1972**, *6*, 4370.
(29) Kim, D. S.; Hohng, S. C.; Malyarchuk, V.; Yoon, Y. C.; Ahn, Y. H.; Yee, K. J.; Park, J. W.; Kim, J.; Park, Q. H.; Lienau, C. *Phys. Rev. Lett.* **2003**, *91*, 143901.